Synthesis, Structure, and Physical Properties of Mixed Valent Mo_2SbS_2, the First Superconducting Antimonide-Sulfide

Chi-Shen Lee,[†] A. Safa-Sefat,[‡] J. E. Greedan,[‡] and Holger Kleinke*,[†]

Department of Chemistry, University of Waterloo, Waterloo, Ontario, Canada N2L 3G1, and Department of Chemistry and the Brockhouse Institute for Materials Research, McMaster University, Hamilton, Ontario, Canada L8S 4M1

Received August 1, 2002. Revised Manuscript Received November 14, 2002

We identified a new ternary molybdenum antimonide-sulfide, Mo_2SbS_2. Black, needle-shaped crystals of Mo_2SbS_2 can be synthesized by reacting stoichiometric amounts of the elements at 850 °C for 7 days with I_2 (<2 wt %) as the transporting reagent; however, the crystals of Mo_2SbS_2 are too small for a single-crystal structure investigation. Therefore, the crystal structure of Mo_2SbS_2 was analyzed by powder X-ray diffraction using Rietveld refinements. The compound crystallizes in a monoclinic system (space group $P2_1/m$, a = 6.50920(7) Å, b = 3.18231(4) Å, c = 9.3548(1) Å, β = 105.4430(8)°, Z = 2). The title compound is isostructural with Mo_2S_3; and the Mo−Mo, Mo−Sb, and Mo−S distances are comparable with those in $MoSb_2S$. The results from the Seebeck coefficient and magnetic susceptibility measurements and electronic band structure calculations suggest metallic behavior. The band structure of Mo_2SbS_2 exhibits van Hove singularities hinting at superconductivity, which was subsequently confirmed via magnetic susceptibility measurements.

Introduction

Thermoelectric materials can be used to convert heat into electricity and vice versa. Today, (doped) binary semiconductors such as Bi_2Te_3, $Si_{0.7}Ge_{0.3}$, and PbTe are used in commercialized systems.[1] In the search for new enhanced thermoelectric materials, several ternary materials are currently being studied, including the filled skutterudites LnM_4Sb_{12} (Ln = lanthanoid, M = Fe, Co, Ni, ...),[2] $CsBi_4Te_6$,[3] and Bi_2Te_3/Sb_2Te_3[4] thin film materials. In general, good thermoelectric materials have a high *figure-of-merit* that combines a high Seebeck coefficient, low thermal conductivity, and high electrical conductivity.[1,5−7]

Our group is focusing on the research into potential thermoelectric materials in ternary transition metal pnictide-chalcogenide systems using both experimental and theoretical approaches. Our synthetic efforts for preparing new thermoelectrics involve the use of heavy main group metalloid elements, such as antimony, selenium, or tellurium, as the common element. Two new ternary molybdenum antimonide-chalcogenides, $MoSb_2Q$ (Q = S, Se),[8,9] have been reported during the course of this study. The title compound Mo_2SbS_2, representing the third compound of this series, was synthesized at high temperatures (T > 850 °C).

The structure of Mo_2SbS_2 contains a two-dimensional building unit, $^2_\infty$[MoSbX], which is topologically equivalent to that of $MoSb_2Q$, but a different interlayer unit, namely $^1_\infty$[MoS] vs $^1_\infty$[Sb] in $MoSb_2Q$. Theoretical investigations (TB-LMTO calculations) point to metallic behavior of Mo_2SbS_2. Interestingly, the band structure analysis clearly shows coexistence of disperse and nearly flat band structures near the Fermi level region (van Hove singularities), which suggests that Mo_2SbS_2 could be a superconductor. This correlation between band structure and superconducting behavior was emphasized in several studies including superconducting cuprates, borocarbides, rare earth carbides, and intermetallic compounds such as $SrSn_3$, Ti_2Sn_3, and $La_{13}Ga_8Sb_{21}$.[10−16] To investigate the possible superconductivity of the title compound as well as other studies,

* To whom correspondence should be addressed. Fax: +1 519-746-0435. E-mail: kleinke@uwaterloo.ca.
[†] University of Waterloo.
[‡] McMaster University.

(1) Rowe, D. M. *CRC Handbook of Thermoelectrics*; CRC Press: Boca Raton, FL, 1995.
(2) Sales, B. C.; Mandrus, D.; Williams, R. K. *Science (Washington, D.C.)* **1996**, *272*, 1325−1328.
(3) Chung, D.-Y.; Hogan, T.; Brazis, P.; Rocci-Lane, M.; Kannewurf, C.; Bastea, M.; Uher, C.; Kanatzidis, M. G. *Science (Washington, D.C.)* **2000**, *287*, 1024−1027.
(4) Venkatasubramanian, R.; Slivola, E.; Colpitts, T.; O'Quinn, B. *Nature (London)* **2001**, *413*, 597−602.
(5) Tritt, T. M., Nolas, G. S., Mahan, G. D., Mandrus, D., Kanatzidis, M. G., Eds.; *Materials Research Society Symposium Proceeding*; Materials Research Society: Warrendale, PA, 2001; Vol. 626.
(6) Tritt, T. M., Kanatzidis, M. G., Mahan, G. D., Lyon, H. B. J., Eds.; *Materials Research Society Symposium Proceeding*; Materials Research Society: Warrendale, PA, 1999; Vol. 545.
(7) DiSalvo, F. J. *Science (Washington, D.C.)* **1999**, *285*, 703−706.
(8) Kleinke, H. *Chem. Commun. (Cambridge)* **2000**, 1941−1942.
(9) Lee, C.-S.; Kleinke, H. *Eur. J. Inorg. Chem.* **2002**, 591−596.
(10) Simon, A.; Yoshiasa, A.; Bäcker, M.; Henn, R. W.; Felser, C.; Kremer, R. K.; Mattausch, H. J. *Z. Anorg. Allg. Chem.* **1996**, *622*, 123−137.
(11) Mattausch, H.; Simon, A.; Felser, C.; Dronskowski, R. *Angew. Chem., Int. Ed. Engl.* **1996**, *35*, 1685−1687.
(12) Hirsch, J. E.; Scalapino, D. J. *Phys. Rev. Lett.* **1986**, *56*, 2732−2735.
(13) Simon, A. *Angew. Chem., Int. Ed. Engl.* **1997**, *36*, 1789−1806.
(14) Fässler, T. F.; Hoffmann, S. *Z. Anorg. Allg. Chem.* **2000**, *626*, 106−112.
(15) Kleinke, H.; Waldeck, M.; Gütlich, P. *Chem. Mater.* **2000**, *12*, 2219−2224.

10.1021/cm020803g CCC: $25.00
Published on Web 01/21/2003

the synthesis, structural characterization, electronic structure, and physical properties of Mo_2SbS_2 will be presented in this paper.

Experimental Section

Synthesis. All starting materials were stored in an argon-filled glovebox. The starting materials were molybdenum powder (Aldrich, 99.9%), antimony powder (Aldrich, 99.8%, melting point 903 K, 99.5%), and sulfur powder (Aldrich, 99.98%). Initial reactions were intended to synthesize $MoSb_2S$. These were carried out by starting from the elements using a small amount of I_2 as transport reagent in a silica tube sealed under vacuum ($<10^{-3}$ mbar). The mixture was heated at 1123 K (850 °C) for 3 days. Black, needle-shape crystals of Mo_2SbS_2 and mixtures of MoS_2 and elemental antimony were found to be present in the reaction mixture. Pure Mo_2SbS_2 can be prepared by heating stoichiometric amounts of the elements at 1173 K for 7 days. Better quality, as well as larger, Mo_2SbS_2 crystals could be synthesized by adding small amounts of I_2 (ca. 30 mg) as the transporting reagent. The purity of Mo_2SbS_2 was checked by powder X-ray diffraction and elemental analyses (EDS). Mo_2SbS_2 is stable in air for at least two weeks. Attempts to synthesize the W and the Se analogues failed.

Structure Determination. Although pure products can be obtained by reacting the Mo/Sb/S reagents in 2:1:2 ratio, single crystals suitable for the structural analyses are very hard to find because of the very small thickness of the needlelike crystals. Typically, the Mo_2SbS_2 reactions yield black, needle-shaped crystals with one long axis (up to 300 μm), and the other two axes usually smaller than 5 μm. Several needle-shaped crystals (in the range of $100 \times 5 \times 5$ μm) were selected under an optical microscope for single-crystal X-ray diffraction experiments and then mounted on glass fibers. In all cases, the first photographs taken on a Bruker APEX CCD diffractometer revealed the presence of very few weak reflections. The best scattering crystal was chosen for the data collection with use of graphite-monochromatized Mo Kα radiation (λ = 0.71073 Å) at 298(2) K. The crystal-to-detector distance was 4.550 cm. Data were collected by a scan of 0.3° in ω in groups of 606 frames each at ϕ settings of 0° and 60°. The exposure time was 120 s/frame. The 2θ values varied between 3° and 70°. The data were corrected for Lorentz and polarization effects.

The data revealed a monoclinic unit cell, and the systematic absences were in agreement with the space groups $P2_1$ and $P2_1/m$. The structure model in the centrosymmetric space group was obtained by direct methods and refined by full-matrix least-squares refinements based on F^2 using the SHELXTL5.12 package.[17,18] This structure solution gave a model isostructural to that of Mo_2S_3, with the formula Mo_2SbS_2. The diffraction data were too weak to give a good structure refinement, with only 45% of the measured reflections being observed (i.e., $I > 2\sigma$).

It was therefore necessary to collect data from a larger crystal, which was later found, again of needlelike shape with a 20-μm diameter. In this case, the scattering power was sufficient, with 76% of the measured reflections having $I > 2\sigma$. Unfortunately, that crystal turned to be an axial twin (along c axis), where of all measured reflections of individual 1, 249 exactly overlapped and 1098 partially overlapped with individual 2, and 637 exhibited no overlap. Deleting all partially overlapped data resulted in a final residual factor of $R(F) = 6.8\%$ and a poor data/parameter ratio of 4:1, whereby the structure model was the same as the one obtained for the weaker, but single crystal.

To obtain final proof for our structure model of Mo_2SbS_2, Rietveld refinements were employed to refine the structure of Mo_2SbS_2 from X-ray powder data. Microcrystalline Mo_2SbS_2 was prepared for powder X-ray diffraction studies. The purity of the Mo_2SbS_2 powder was checked by a Bruker D500 X-ray powder diffractometer, and then the data for Rietveld refinement were collected on an Inel powder X-ray diffractometer. The diffraction data were collected simultaneously with a position-sensitive detector (CPS590; 500-mm radius, 90° detection angle) at room temperature for 7 h. The data were analyzed using the GSAS software system.[19,20] The 2θ range for the refinements was set between 2.0° and 90°. The starting structural model of Mo_2SbS_2 was taken from the results of the single-crystal X-ray diffraction study. Refined structural parameters included overall scale factors, lattice parameters, fractional coordinates, anisotropic thermal displacement parameters, and site occupancies. Absorption parameters and an extinction coefficient were also refined. Backgrounds were fitted using a 30-parameter analytical function, and peak shapes were fitted using exponential pseudo-Voigt functions.[19] After the structure of the main phase was determined, refinements including impurities from the starting elements and possible binary phases were included. The products of the Mo_2SbS_2 reaction include trace amounts of Sb, MoS_2, and MoO_2 (less than 2%). The experimental and Rietveld refined profiles of these data are shown in Figure 1. No significant change in site occupancies (<2%) occurred for any atoms during the refinement, and all atoms exhibit reasonable thermal displacement parameters. Summaries of the crystallographic data and refinement, atomic positions and isotropic displacement parameters, and interatomic distances for each sample are listed in Tables 1−3. No evidence for a significant phase range was found; deviations from the ideal stoichiometry Mo_2SbS_2 resulted in a mixture of phases, e.g. Mo_2S_3 and Mo_2SbS_2 in the S-rich region.

Elemental Analysis. Energy dispersive spectroscopy (EDS, LEO 1050) was performed on the crystalline and powdered

Table 1. Crystal Data and Conditions of Data Collection for Mo_2SbS_2

refined composition	Mo_2SbS_2
instrument	Inel powder X-ray diffractometer
formula weight [g/mol]	371.5
crystal system	monoclinic
space group, Z	$P2_1/m$, 2
a [Å]	6.50920(7)
b [Å]	3.18231(4)
c [Å]	9.3548(1)
β	105.4430(8)°
V [Å^3]	186.782(4)
$2\theta_{max}$	90°
detector	CPS590
radiation (Å)	Cu Kα_1, 1.54056
data points	7155
structural refinements	GSAS
profile functions	pseudo-Voigt
R_p, R_{wp} (%)[a]	6.28, 7.91
goodness-of-fit (χ)[b]	1.55
variable parameters	111

[a] $R_p = \sum||Y_o| - |Y_c||/\sum|Y_o|$; $R_{wp} = [\sum[w(Y_o^2 - Y_c^2)^2]/\sum[w(Y_o^2)^2]]^{1/2}$; Y_o and Y_c are observed and calculated counts. [b] $\chi = [\sum[w(Y_o^2 - Y_c^2)^2]/(N_{obs} - N_{var})]^{1/2}$; N_{obs} is the number of observations and N_{var} is the number of parameters.

Table 2. Atomic Positions and Displacement Parameters for Mo_2SbS_2 (Refined from Powder X-ray Diffraction)

atom	site	x	y	z	U_{eq} [×100 Å^2][a]
Mo1	2e	0.6645(3)	0.25	0.4802(2)	0.54(8)
Mo2	2e	0.8943(3)	0.25	0.8857(2)	0.63(8)
Sb	2e	0.9971(3)	0.25	0.3378(2)	0.85(7)
S1	2e	0.5260(1)	0.25	0.6933(8)	0.4(2)
S2	2e	0.2783(9)	0.25	0.9891(8)	0.9(2)

[a] $U_{eq} = (1/3)\sum_i \sum_j U_{ij} a^i a^j a_i a_j$.

(16) Mills, A. M.; Deakin, L.; Mar, A. *Chem. Mater.* **2001**, *13*, 1778−1788.
(17) *SAINT Version 4*; Siemens Analytical X-ray Instruments Inc.: Madison, WI, 1995.
(18) *SHELXTL Version 5.12*; Reference Manual, Siemens Analytical X-ray Systems, Inc.: Madison, WI, 1995, 1996.
(19) Von Dreele, R. B.; Jorgensen, J. D.; Windsor, C. G. *J. Appl. Crystallogr.* **1982**, *15*, 581−589.
(20) Larson, L. C.; Von Dreele, R. B.; *LANSCE*, MSH805; Los Alamos National Laboratory: Los Alamos, NM, 1995.

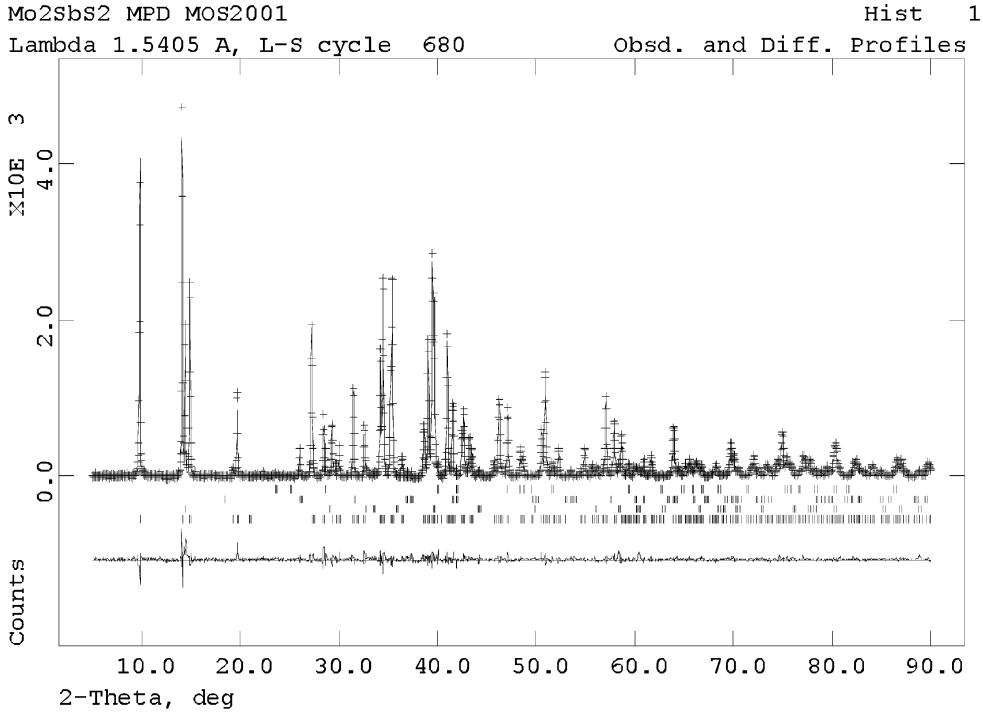

Figure 1. Observed (cross spots), calculated (solid line), and difference plots (button) for X-ray powder profile of the Mo_2SbS_2 from Rietveld refinements. The vertical marks from top to button are the Bragg angle positions for Sb, MoS_2, MoO_2, and Mo_2SbS_2, respectively.

Table 3. Selected Bond Lengths [Å] for Mo_2SbS_2

Mo1	Mo1 (×2)	3.18231(4)
	Mo1 (×2)	2.771(3)
	Sb3 (×3)	2.828(3)
	S4 (×1)	2.398(7)
	S4 (×2)	2.373(5)
Mo2	Mo2 (×2)	3.18231(4)
	Mo2 (×2)	2.726(3)
	Sb3 (×2)	2.862(2)
	S4 (×1)	2.587(7)
	S5 (×2)	2.401(6)
	S5 (×1)	2.406(5)
Sb3	Sb3 (×2)	3.18231(4)
	Sb3 (×2)	3.418(3)

samples. Although the Mo:S ratio cannot be determined because of the severe overlap of the peaks of Mo (Lα = 2.293 eV) and S (Kα = 2.307 eV), the three desired elements Mo, Sb, and S were definitely present with a homogeneous distribution in all cases. No impurities of other elements (like iodine or silicon) were detected.

Thermopower Measurements. Seebeck coefficients were determined on a cold-pressed bar by a commercial thermopower measurement apparatus (MMR Technologies) in the temperature range between 300 and 600 K, using Constantan as an internal standard. Silver paint (AMI DODUCO Technology) was used to create electric contacts.

Magnetic Susceptibility Measurements. The temperature-dependent magnetization was carried out on a Quantum Design MPMS superconducting quantum-interference device (SQUID). The zero-field-cooled (ZFC) and field-cooled (FC) DC susceptibilities were measured from 1.8 to 12 K for the Mo_2SbS_2 sample. For the ZFC measurements, the sample was first cooled from room temperature to 1.8 K in zero applied field (H_a); the susceptibility was subsequently measured during warming at $H_a = 100$ G. For the FC measurements, the sample was cooled from room temperature to 1.8 K while at 100 G. The susceptibility was then measured at the same applied field during warming of the sample up to room temperature.

Electronic Structure Calculations. The tight-binding linear muffin tin orbitals (LMTO)[21−23] band calculations were carried out to understand the electronic structure of Mo_2SbS_2. The integration in k space was performed by an improved tetrahedron method on a grid of 12 × 24 × 6 unique k points of the first Brillouin zone (i.e., 494 of 1728 k points).[24] We analyzed the electronic structure by extracting information from the band structure, densities of states (DOS), and crystal orbital Hamilton population curves (COHP).[25]

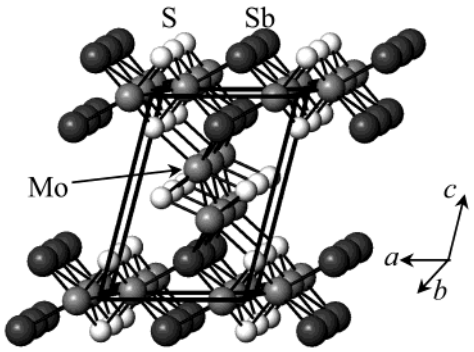

Figure 2. Crystal structure of Mo_2SbS_2 in a projection along [010]. Medium gray circles, Mo; large dark circles, Sb; bright circles, S atoms. The origin has been translated by 1/2, 1/2, 1/2, to line up the MoSbS layers with the a axis.

Results and Discussion

Crystal Structure. Mo_2SbS_2 crystallizes in the space group $P2_1/m$, with five independent positions: two for Mo, one for Sb, and two for S atoms. The structure consists of two-dimensional layers of β-$MoTe_2$-related building blocks, $^2_\infty$[MoSbS], parallel to the ab-plane, and one-dimensional chains, $^1_\infty$[MoS], along the b axis, which connect to form a three-dimensional network as shown in Figure 2.

(21) Andersen, O. K. *Phys. Rev. B* **1975**, *12*, 3060−3083.
(22) Skriver, H. L. *The LMTO Method*; Springer: Berlin, 1984.
(23) Hedin, L.; Lundqvist, B. I. *J. Phys. C* **1971**, *4*, 2064−2083.
(24) Blöchl, P. E.; Jepsen, O.; Andersen, O. K. *Phys. Rev. B: Condens. Matter* **1994**, *49*, 16223−16233.
(25) Dronskowski, R.; Blöchl, P. E. *J. Phys. Chem.* **1993**, *97*, 8617−8624.

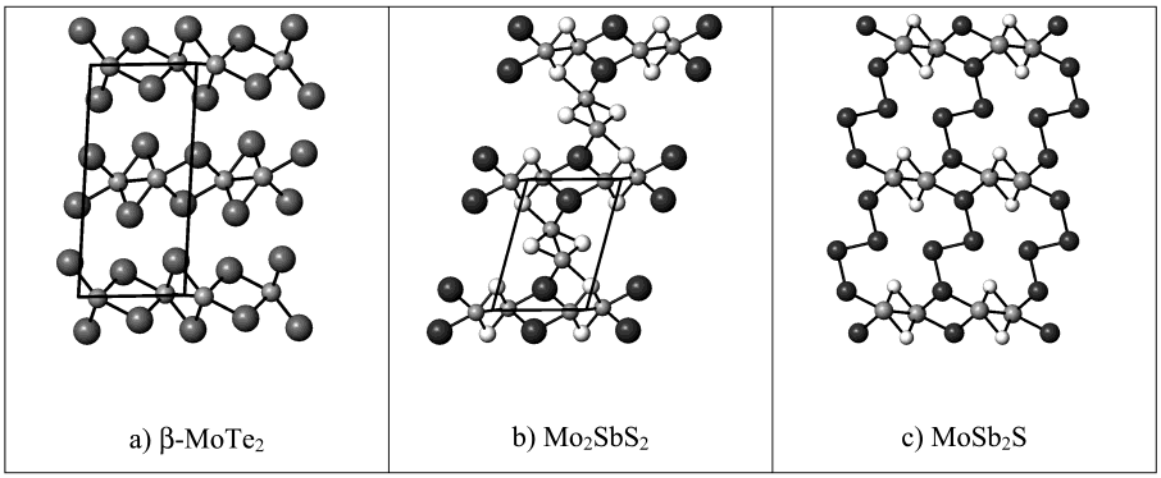

Figure 3. Crystal structures of (a) β-$MoTe_2$, (b) Mo_2SbS_2, and (c) $MoSb_2S$. Medium gray circles, Mo; large dark circles, Sb/Te; bright circles, S atoms.

Each $^2_\infty$[MoSbS] layer is constructed from two approximately closest-packed sheets consisting of the Sb and S atoms with the Mo1 atom located in the pseudo octahedral sites. The Mo1 atoms within the $^2_\infty$[MoSbS] layer form zigzag chains along the *b* axis. The Mo1−Mo1 distances are 2.77 and 3.18 Å within the Mo1 zigzag chain and 4.56 Å between two adjacent chains in the $^2_\infty$[MoSbS] layer. Each Mo1 atom is coordinated by three Sb and three S atoms in a distorted octahedral site (d_{Mo-Sb} = 2.83, 2.88 Å; d_{Mo-S} = 2.40, 2.37 Å). Such a layered building block is also present in the structures of $MoSb_2X$ (X = S, Se).[8,9] The short Mo1−Mo1 distances are essentially the same as those in $MoSb_2S$ (d_{Mo-Mo} = 2.77 Å), thus shorter than those in Mo_2S_3[26] (d_{Mo-Mo} = 2.85 Å). A structural comparison of β-$MoTe_2$,[27] Mo_2SbS_2, and $MoSb_2S$[9] is given in Figure 3.

The other building block, $^1_\infty$[MoS], is located between two $^2_\infty$[MoSbS] layers. It comprises Mo2 zigzag chains. Each Mo2 atom is bonded to two Sb and one S atoms from $^2_\infty$[MoSbS] layer and three S atoms within the $^1_\infty$[MoS] chain in a distorted octahedral site (d_{Mo-Sb} = 2.86 Å; d_{Mo-S} = 2.59, 2.40, 2.41 Å). The Mo2 chains are roughly parallel to the (101) plane and perpendicular to the Mo1 chain in the *ab*-plane. The Mo2−Mo2 distances are 2.73 and 3.18 Å, respectively, significantly shorter than the corresponding Mo−Mo distances in Mo_2S_3 (2.85, 3.20 Å).

Moreover, the interchain Mo1−Mo2 distance is 3.69 Å, which is much longer than the corresponding interchain distance in Mo_2S_3 (3.23 Å). This indicates that there is essentially no interchain Mo−Mo interaction in Mo_2SbS_2; on the other hand, the Mo1−Mo2 interactions in Mo_2S_3 cannot be ignored. Overall, the average Mo−Mo bonds of 2.75 Å in Mo_2SbS_2 are typical for strong Mo−Mo bonds, as comparisons with elemental molybdenum (cubic body-centered, 2.73 Å), β-$MoTe_2$ (2.89 Å), Mo_2S_3 (2.85 Å), and $MoSb_2S$ (2.76 Å) reveal. The averaged Mo−Sb and Mo−S distances are 2.86 and 2.44 Å, which may be compared to the corresponding interatomic distances in $MoSb_2S$ (d_{Mo-Sb} = 2.84 and d_{Mo-S} = 2.38 Å) and Mo_2S_3 (d_{Mo-S} = 2.41 Å). The shortest Sb−Sb distance within the $^2_\infty$[MoSbS] layer is 3.18 Å, comparable to the analogous Sb−Sb contact in $MoSb_2S$ (d_{Sb-Sb} = 3.19 Å). Such Sb−Sb contacts are longer than a regular Sb−Sb single bond (2.80−2.90 Å), but shorter than the weak bond in elemental antimony (d = 3.35 Å), and have often been classified as half bonds.[28−32]

To a first approximation, the formal charges of each atom in Mo_2SbS_2 may be assigned qualitatively based on the Zintl−Klemm concept. Among these elements, the electronegativity of sulfur is the largest on any electronegativity scale so that S can be treated as S^{2-} ions. The formal charge of the Sb atom may be assigned as Sb^{2-}, assuming there are two-half bonds along the *b* axis. To balance the charge from Sb and S, the charge of the Mo atoms would then be 3+ (d^3 configuration), the same as the formal charge of the Mo atom in Mo_2S_3. However, the different coordination environments of Mo1 and Mo2 and the differences in Mo−Mo bonding, compared to Mo_2S_3, stand against an assignment of Mo^{3+}. The Mo−Mo bonds are of the same length as in $MoSb_2S$, which involves Mo^{4+}. We will therefore give a more detailed discussion based on the results from the band structure calculations in the next section.

Electronic Structure. The TB-LMTO band calculations were employed to calculate the electronic structure of Mo_2SbS_2 to understand its physical properties and interatomic interactions. Density of states (DOS) curves for Mo_2SbS_2 and the partial projections onto the Mo, Sb, and S orbitals are illustrated in Figure 4. At low energy (below −8 eV) the densities of states are dominated by the S *s* and Sb *s* orbitals. The S *s* and Sb *s* blocks occur in the energy windows between −13 and −15 eV and −7 and −12 eV, respectively. The broad peak between −8 eV and the Fermi level at 0 eV is mostly made up of S *p*, Sb *p*, and Mo *d* orbitals, used for Mo−Mo, Mo−S, Mo−Sb, and Sb−Sb interactions. The states near the Fermi level comprise mainly Mo *d*

(26) Schutte, W. J.; Disselborg, F.; de Boer, J. L. *Acta Crystallogr.* **1993**, *B49*, 787−794.
(27) Brown, B. E. *Acta Crystallogr.* **1966**, *20*, 268−274.
(28) Bolloré, G.; Ferguson, M. J.; Hushagen, R. W.; Mar, A. *Chem. Mater.* **1995**, *7*, 2229−2231.
(29) Kleinke, H. *Eur. J. Inorg. Chem.* **1998**, 1369−1375.
(30) Kleinke, H. *J. Am. Chem. Soc.* **2000**, *122*, 853−860.
(31) Kleinke, H. *Chem. Soc. Rev.* **2000**, *29*, 411−418.
(32) Papoian, G. A.; Hoffmann, R. *Angew. Chem., Int. Ed.* **2000**, *39*, 2408−2448.

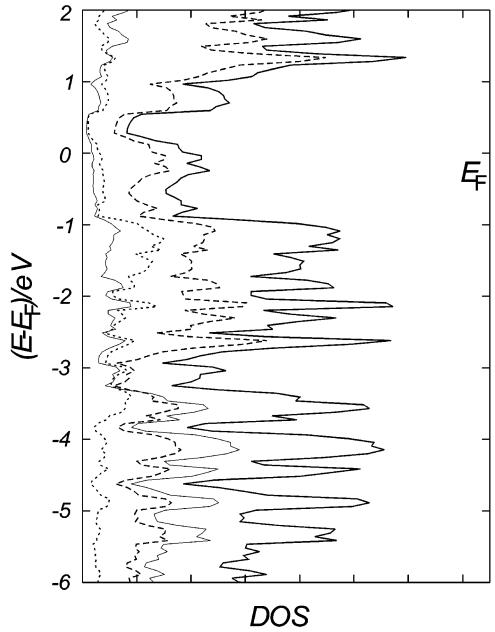

Figure 4. Density of states (DOS) curves for Mo_2SbS_2. The horizontal dashed line denotes the Fermi energy (E_F). Thick solid line, total DOS; dashed line, Mo; thin solid line, Sb; dotted line, S contributions.

orbitals, whereas the contributions from the Sb and S atoms are much smaller. There is no band gap, but a significant local maximum of the DOS curve at the Fermi level, to which the Mo d_{z^2} orbital contributes most dominantly (see band structure). The existence of nonzero electronic states at the Fermi level suggests metallic behavior for Mo_2SbS_2.

The interatomic interactions in Mo_2SbS_2 were analyzed by integrating over the COHP curves up to the Fermi level, resulting in ICOHP values as a function of the relative energy. This is a similar procedure to obtaining the (probably better known) Mulliken overlap populations (MOPs)[33] from the crystal orbital overlap population (COOP) curves calculated with the extended Hückel method,[34−36] with the COHP curves basically supplying information comparable to the COOP curves. Bonding interactions correspond to negative values of ICOHPs, in contrast to MOPs, where stronger bonds exhibit higher positive values. The COHP curves for the Mo−S and Mo−Sb interactions are shown in Figure 5a. Strong Mo−Sb and Mo−S bonding is evident, with major contributions between −1 and −5 eV for the Mo−Sb and −3 and −8 eV for the Mo−S interactions. The Mo−Sb and Mo−S bonds are essentially optimized at the Fermi level (ICOHP values: Mo−Sb = −1.69; Mo−S = −2.93 eV per bond). The Sb−Sb interactions (Figure 5a) that represent the Sb−Sb contacts within the $^2_\infty$[MoSbS] layer (d_{Sb-Sb} = 3.18 Å) exhibit antibonding character at the Fermi level, yet overall bonding character with an average ICOHP value of −0.53 eV/bond. The Sb−Sb interaction in the $^2_\infty$[MoSbS] layer is comparable with the Sb−Sb contacts in the similar layer in $MoSb_2S$ (d_{Sb-Sb} = 3.19 Å; ICOHP = −0.41 eV/bond).

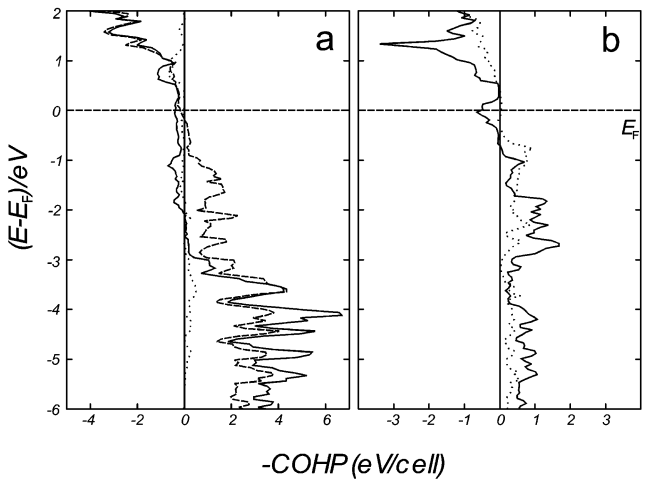

Figure 5. Cumulated crystal orbital Hamilton (COHP) curves for (a) Mo−Sb (solid line), Mo−S (dashed line), and Sb−Sb (dotted line); (b) Mo1−Mo1 (solid line) and Mo2−Mo2 (dotted line).

Such a Sb−Sb interaction could be considered as a half bond at best, probably even less than that because of its nonzero ICOHP value compared with the full bonds in KSb[37] with larger ICOHPs of −2.29 and −1.87 eV/bond. Similar values were also found for the long Sb−Sb contacts in elemental antimony (d_{Sb-Sb} = 3.35 Å; ICOHP = −0.23 eV/bond), Mo_3Sb_7[38] (d_{Sb-Sb} = 3.10 Å; ICOHP = −0.23 eV/bond), and $Zr_{11}Sb_{18}$[39] (d_{Sb-Sb} = 3.11 Å; ICOHP = −0.49 eV/bond).

The COHP curves for the two Mo−Mo interactions shorter than 2.8 Å (Mo1−Mo1 and Mo2−Mo2) are shown in Figure 5b. At the Fermi level (E_F), only the Mo1−Mo1 interaction exhibits antibonding character, with an ICOHP value (−1.14 eV/bond) significantly lower than that of the Mo2−Mo2 contacts (ICOHP = −1.92 eV/bond). The ICOHP values of the Mo−Mo interactions point to different electronic configurations of Mo1 and Mo2. A comparison with ICOHP values of Mo_2S_3, Mo_2SbS_2, and $MoSb_2S$ is given in Table 4. The ICOHP value of Mo1−Mo1 interaction is similar to that of the Mo−Mo interaction in Mo_2S_3, whereas the ICOHP value of Mo2−Mo2 interaction is close to that of $MoSb_2S$. Although the Mo−Mo distances of Mo1 and Mo2 are comparable, their coordination environments are quite different (Mo1, 3Sb + 3S; Mo2, 2Sb + 4S). This apparently leads to a mixed valent compound based on the ICOHP values, with Mo1 being similar to the Mo^{3+} in Mo_2S_3 and Mo2 being similar to the Mo^{4+} in $MoSb_2S$. As mentioned before, the Sb−Sb contacts in Mo_2SbS_2 clearly exhibit bonding character; therefore, the formal charge of Sb is between −3 (zero bonds) and −2 (two-half bonds). The overall result is thus $Mo^{+3+\alpha}Mo^{+4+\beta}$-$Sb^{-3+\gamma}(S^{2-})_2$ ($\alpha + \beta + \gamma = 0$; $\alpha > 0$, $\beta < 0$, $\gamma > 0$).

The band structure along selected paths of the first Brillouin zone[40] is shown in Figure 6, with the fat bands emphasizing the contribution of the Mo2 d_{z^2} orbitals. The band structure of Mo_2SbS_2 features large dispersive

(33) Mulliken, R. S. *J. Chem. Phys.* **1955**, *23*, 2343−2346.
(34) Hughbanks, T.; Hoffmann, R. *J. Am. Chem. Soc.* **1983**, *105*, 3528−3537.
(35) Hoffmann, R. *J. Chem. Phys.* **1963**, *39*, 1397−1412.
(36) Whangbo, M.-H.; Hoffmann, R. *J. Am. Chem. Soc.* **1978**, *100*, 6093−6098.
(37) Hönle, W.; von Schnering, H.-G. *Z. Kristallogr.* **1981**, *155*, 307−314.
(38) Dashjav, E.; Szczepenowska, A.; Kleinke, H. *J. Mater. Chem.* **2002**, *12*, 345−349.
(39) Elder, I.; Lee, C.-S.; Kleinke, H. *Inorg. Chem.* **2002**, *41*, 538−545.
(40) Kokalj, A. *J. Mol. Graph. Model.* **1999**, *17*, 176−179.

Table 4. Summary of Bond Distances and ICOHP Values for Various Interatomic Contacts in Mo_2S_3, Mo_2SbS_2, and $MoSb_2S$

	Mo_2S_3		Mo_2SbS_2		$MoSb_2S$	
	d(Å)	ICOHP (eV/bond)	*d*(Å)	ICOHP (eV/bond)	*d*(Å)	ICOHP (eV/bond)
$^2_\infty$[MoSbS]						
Mo1−Mo1	2.85	−1.70	2.75	−1.14	2.76	−1.90
Mo1−Mo1	3.23	−0.76	3.18	−0.27	3.19	−0.68
Mo1−S	2.37	−2.99	2.30	−2.86	2.38	−2.99
Mo1−Sb			2.84	−1.22	2.83	−1.77
Sb−Sb			3.41	−0.15	3.33	−0.11
			3.18	−0.53	3.19	−0.41
interlayer						
Mo1−Mo2 interchain	3.23	−0.37	3.62	−0.09		
Mo−Sb			2.83	−0.95		
Mo−S	2.57	−1.22	2.67	−1.36		
S−S	3.20		3.40			
$^1_\infty$[MoS]						
Mo2−Mo2	2.85	−0.94	2.75	−1.92		
Mo2−Mo2	3.20	−0.29	3.18	−0.54		
Mo−S	2.35	−2.18	2.38	−2.99		

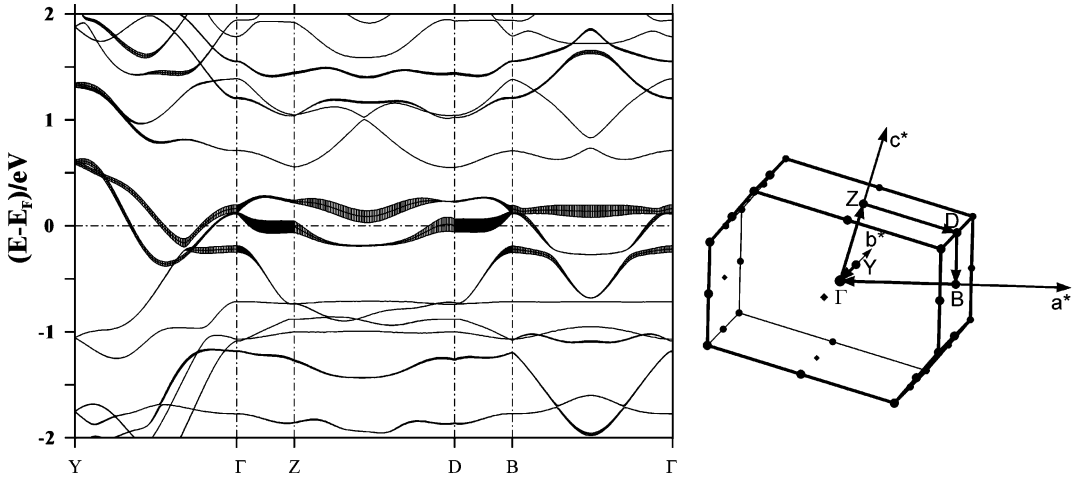

Figure 6. Band structure of Mo_2SbS_2. The dashed line denotes the Fermi energy. The interlayer Mo d_{z^2} contributions are emphasized.

bands crossing E_F that reveal metallic properties as well as flat bands at E_F that are not present in the band structure of Mo_2S_3 (both from LMTO (our work) as well as extended Hückel[41,42] calculations). Bands crossing the Fermi level along Y−Γ and B−Γ (parallel to *b** and *a**) correspond to Mo−Mo (within the zigzag chains) and Mo−Sb interactions.

The flat bands along Γ−Z and D−B exhibit a very narrow dispersion (less than 0.1 eV), which are dominated by Mo2 d_{z^2} contributions related to the interchain Mo−Mo interactions. These contributions indicate electronic states with localized electron pairs near the Fermi level. The coexistence of steep bands (fast delocalized electrons) as well as flat bands (localized electron pairs) near the Fermi level is considered as a fingerprint for superconducting behavior (van Hove singularity).[13−15,43,44] Therefore, we performed further investigations to check for superconductivity, namely magnetic susceptibility experiments.

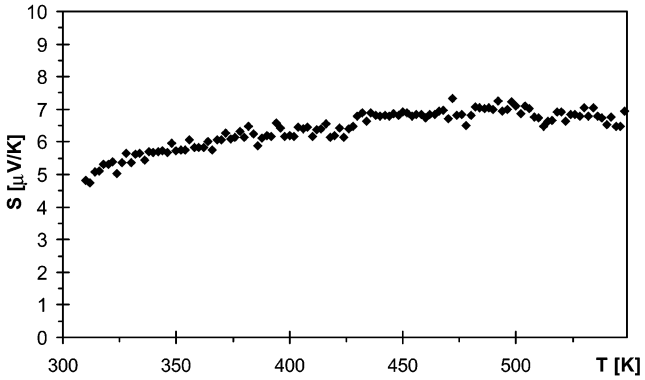

Figure 7. Temperature-dependent Seebeck coefficients of Mo_2SbS_2.

Physical Properties. *Seebeck Measurements.* The temperature-dependent Seebeck coefficient measurement is shown in Figure 7. The Seebeck coefficient *S* remains between +5 and +10 μV/K over the temperature range from 300 to 600 K. The positive sign indicates that holes are the dominating charge carriers (p-type thermoelectric material). Typical magnitudes of Seebeck coefficients at 300 K range from a few μV/K for most metals to 10−20 μV/K for some transition metal ele-

(41) Whangbo, M. H.; Canadell, E. *J. Am. Chem. Soc.* **1992**, *114*, 9587−9600.
(42) Canadell, E.; LeBeuze, A.; El Khalifa, M. A.; Chevrel, R.; Whangbo, M. H. *J. Am. Chem. Soc.* **1989**, *111*, 3778−3782.
(43) Köckerling, M.; Johrendt, D.; Finckh, E. W. *J. Am. Chem. Soc.* **1998**, *120*.
(44) Fässler, T. F.; Hoffmann, S.; Kronseder, C. *Z. Anorg. Allg. Chem.* **2002**, *627*, 2486-2492.

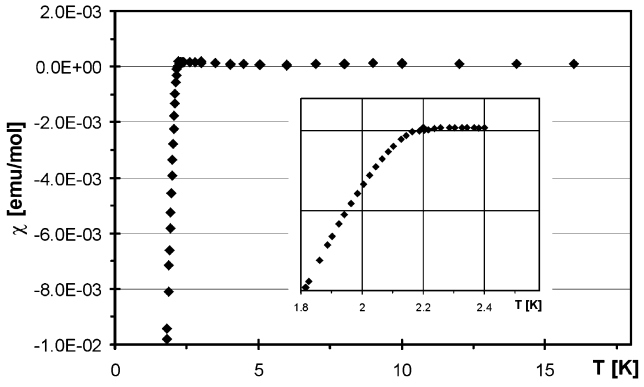

Figure 8. Magnetic susceptibility measurements of Mo_2SbS_2.The inset emphasizes the phase transition.

ments. The observed Seebeck coefficient of Mo_2SbS_2 is of the same order as most metallic materials.

Magnetic Susceptibility Measurements. The ZFC susceptibilities (not corrected for diamagnetic contributions) of Mo_2SbS_2 are shown in Figure 8. Mo_2SbS_2 exhibits temperature-independent Pauli paramagnetism between 300 and 2.2 K that outweighs the diamagnetic contributions, which is typical for a metallic material. The ZFC magnetization curve displays a transition temperature T_c at 2.20 K (see inset); below T_c strong diamagnetism (flux expulsion) is evident. This can be explained with a transition to the superconducting state, i.e., a metal to superconductor transition. Because of the temperature limits of our equipment, it was not possible to determine the saturation magnetization. The parent compound Mo_2S_3, with the Mo atoms having d^3 configuration, itself exhibits two phase transitions associated with symmetry reductions caused by different Mo atom ordering, namely at 182 and 145 K.[45]

(45) Rashid, M. H.; Sellmyer, D. J.; Katkanant, V.; Kirby, R. D. *Solid State Commun.* **1982**, *43*, 675−678.

Conclusion

In summary, the syntheses and characterization of a new ternary compound, Mo_2SbS_2, were presented. Mo_2SbS_2 crystallizes in ternary ordered variant of Mo_2S_3, exhibiting $^2_\infty$[MoSbS] layers and $^1_\infty$[MoS] chains. The structure comprises strong heteronuclear Mo−S and Mo−Sb, strong homonuclear Mo−Mo and intermediate Sb−Sb interactions. The Mo−Mo interactions can be correlated with the Mo−Mo interactions in Mo_2S_3 and $MoSb_2S$. Mo_2SbS_2 exhibits metallic behavior as predicted by electron counting, electronic structure calculations, and confirmed by physical property measurements (small Seebeck coefficients and Pauli paramagnetism). The results from the electronic structure calculations suggest different electronic configurations of Mo1 and Mo2, i.e., a mixed valent compound. This is in contrast to Mo_2S_3, which undergoes metal/nonmetal transitions upon cooling due to the d^3 configuration. Band structure analyses revealed a van Hove singularity, indicating superconducting behavior of Mo_2SbS_2. This assumption has been confirmed by magnetic susceptibility measurements, which revealed a transition to the superconducting state at 2.2 K.

Acknowledgment. Financial support from the Canada Foundation for Innovation, the Canada Research Chair Secretariat, the Ontario Innovation Trust, Materials Manufacturing Ontario, the Natural Sciences and Engineering Research Council of Canada, and the Province of Ontario (Premier's Research Excellence Award for H.K.) is appreciated. We are indebted to Henry Pilliere (Inel) for the X-ray powder data collection.

Supporting Information Available: Table of anisotropic displacement parameters for $MoSb_2S$. This material is available free of charge via the Internet at http://pubs.acs.org.

CM020803G